Biophysical Chemistry 296 (2023) 107002

Contents lists available at ScienceDirect

Biophysical Chemistry

journal homepage: www.elsevier.com/locate/biophyschem

Interaction of detergent with complex mimics of bacterial membranes

Nadine Angerer [a,b,c], Paulina Piller [a,b,c], Enrico F. Semeraro [a,b,c], Sandro Keller [a,b,c], Georg Pabst [a,b,c,*]

[a] Biophysics, Institute of Molecular Bioscience (IMB), NAWI Graz, University of Graz, Humboldtstr. 50/III, Graz 8010, Austria
[b] BioTechMed Graz, Graz, Austria
[c] Field of Excellence BioHealth – University of Graz, Graz, Austria

ARTICLE INFO

Keywords:
Isothermal titration calorimetry
Phase diagram
Lipid mixtures
Spontaneous monolayer curvature

ABSTRACT

Detergents are valuable tools to extract membrane proteins for biophysical, biochemical, and structural scrutiny. The detergent-driven solubilization of bilayers made from a single lipid species is commonly described in terms of pseudo-phase diagrams and a three-stage model accounting for three ranges comprising (i) intact vesicles, (ii) vesicle/micelle co-existence, or (iii) mixed micelles. Moreover, the pseudo-phase boundaries thus determined can often be quantitatively rationalized in terms of the molecular shapes of the lipid and the detergent used. Yet, it has remained unclear to what extent this approach can be applied to multi-component lipid membranes that more closely mimic the compositional complexity of cellular membranes. Here, we studied how lipid mixtures composed of palmitoyl oleoyl phosphatidylethanolamine (POPE), palmitoyl oleoyl phosphatidylglycerol (POPG), and tetraoleoyl cardiolipin (TOCL) are solubilized by the commonly used zwitterionic detergent lauryldimethylamine *N*-oxide using isothermal titration calorimetry. While phase diagrams of the diverse lipid mixtures showed the typical ranges of the three-stage model, we found that POPG-rich POPE/POPG bilayers are more difficult to solubilize than POPG-poor POPE/POPG bilayers. In turn, POPE/POPG/TOCL bilayers became increasingly resistant to detergent with increasing TOCL content. Since POPG is nearly cylindrically shaped and TOCL adopts inverted cone-like shapes under current buffer conditions, our solubilization data do not align with shape-based arguments. Instead, additional electrostatic interactions between lipids and detergents lead to non-additive mixing behavior affecting the resilience of complex lipid bilayers against solubilization.

1. Introduction

Elucidating the structures and functions of membrane proteins remains one of the largest challenges in the life sciences. Common strategies for gaining insights into the structures and functions of membrane proteins involve isolating the protein of interest from its native membrane and reconstituting it into synthetic lipid bilayers of well-defined composition [1,2]. Traditionally, detergents have been widely exploited for this purpose [3]. Recently, polymer-based nanodiscs have attracted significant attention for membrane-protein extraction while avoiding the need to remove the protein from its native lipid environment [4–6]. Still, detergents are often used for membrane-protein extraction prior to reconstitution into lipid vesicles [7].

The choice of model membrane into which membrane proteins are reconstituted is delicate and requires balancing experimental tractability with physiological relevance. This aspect is particularly subtle in view of the large body of evidence for both specific and unspecific interactions between lipids and proteins [8–10]. That is, membrane-protein function in general depends on the lipid composition of the chosen synthetic membrane. For example, different proteolytic activities were recently reported for an integral enzyme in phosphatidylcholine and phosphatidylethanolamine/phosphatidylglycerol bilayers [11]. Of particular interest is the use of lipid mixtures for more advanced mimics of natural membranes [12]. However, only little is known about the interactions of detergents with lipid mixtures. Mostly such research efforts are focused on the differential solubilization of mixtures forming cholesterol-enriched lipid domains (for review see, e.g. [13]).

Two previous reports addressed the detergent-induced vesicle-to-micelle transition in binary mixtures of zwitterionic and anionic phospholipids [14,15]. The observed behavior was in good agreement with the three-stage model put forward by Helenius and Simons [16]. According to this model, detergent-lipid phase diagrams are described in

* Corresponding author at: Biophysics, Institute of Molecular Bioscience (IMB), NAWI Graz, University of Graz, Humboldtstr. 50/III, Graz 8010, Austria.
E-mail address: georg.pabst@uni-graz.at (G. Pabst).

https://doi.org/10.1016/j.bpc.2023.107002
Received 10 January 2023; Received in revised form 2 March 2023; Accepted 2 March 2023
Available online 8 March 2023

terms of pseudo-phases comprising (i) the vesicle range, where detergent partitions into the bilayer phase, (ii) the coexistence range containing both mixed micelles and vesicles, and (iii) the micellar range, where all vesicles are fully dissolved and only mixed micelles of varying lipid-detergent composition are left. Both of the above-mentioned studies on lipid mixtures report that the molecular shapes of lipid and detergent—and the resulting spontaneous monolayer curvatures—are the dominant contributions governing the transformation of vesicles into micelles [14,15]. In brief, detergents impose positive spontaneous monolayer curvature stress upon partitioning into the lipid membranes, leading to their destabilization [17]. Such shape-based arguments are simple yet powerful tools to rationalize the vesicle-to-micelle transition and, therefore, are broadly applied to interpreting the thermodynamics of detergent/lipid mixtures [13].

Here, we studied interactions of palmitoyl phosphatidylethanolamine (POPE), palmitoyl phosphatidylglycerol (POPG), and tetraoleoyl cardiolipin (TOCL) mixtures with the zwitterionic detergent lauryldimethylamine *N*-oxide (LDAO). All three phospholipids are abundant in bacteria [18] and, thus, are frequently used to mimic bacterial membranes (see, e.g. [19,20]). Applying isothermal titration calorimetry (ITC), we derived the phase diagrams of LDAO-POPE/POPG and LDAO-POPE/POPG/TOCL mixtures over a broad range of lipid compositions.

In general, we find that POPE/POPG/TOCL bilayers are more resilient to LDAO than POPE/POPG mixtures. Moreover, increasing the TOCL content in POPE/POPG/TOCL mixtures, i.e., increasing negative monolayer spontaneous curvature contributions, further enhances this resilience. Strikingly, the stability of POPE/POPG membranes also increased with increasing POPG content, i.e., upon shifting spontaneous monolayer curvatures toward positive values. Our results thus do not align with commonly accepted shape-based arguments for detergent-lipid interactions. Instead, it appears that more complex interactions, presumably of electrostatic nature, would additionally need to be considered.

2. Materials and methods

2.1. Sample preparation

POPE, POPG, and TOCL were obtained from Avanti Polar Lipids (Birmingham, AL) and were used without further purification. LDAO was from GLYCON Biochemicals (Luckenwalde, Germany); see Fig. 1 for the corresponding chemical structures. All other chemicals, including tris(hydroxymethyl)aminomethane (TRIS), ethylenediaminetetraacetic acid (EDTA), NaCl, $CHCl_3$, and CH_3OH were purchased from Carl Roth (Karlsruhe, Germany) in *pro analysis* quality.

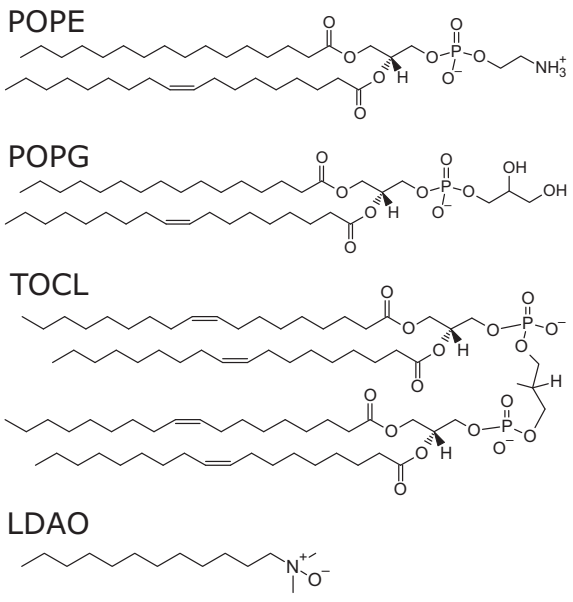

Fig. 1. Chemical structures of all lipids and the detergent used in this study.

Stock solutions were prepared by dissolving weighed amounts of lipids in $CHCl_3/CH_3OH$ (9:1 vol/vol), and aliquots thereof were mixed to obtain the desired phospholipid molar ratios. These solutions were subsequently dried using a gentle stream of N_2, followed by incubation in vacuum for at least 8 h. Large unilamellar vesicles (LUVs) were obtained by (i) dispersing the dry lipid films in buffer solutions using intermittent vigorous vortex mixing at room temperature followed by (ii) passing the lipid dispersions 31 times through polycarbonate filters (pore size: 100 nm) using a hand-held mini-extruder (Avanti Polar Lipids). All lipid mixtures were dispersed in Tris-EDTA (TE) buffer (20 mM Tris, 2 mM EDTA, pH 8.3). Lipid concentrations of stock solutions and LUV dispersions were determined using a phosphate assay [21]. Formation of LUVs with a narrow size distribution was monitored by dynamic light scattering using a Zetasizer Nano ZSP (Malvern Panalytical, Worcestershire, UK).

2.2. Differential scanning calorimetry (DSC)

DSC measurements were performed using a Nano-DSC high-sensitivity differential scanning calorimeter (TA Instruments, New Castle, DE). Scans of 1 mg/mL lipid concentration were recorded at a constant rate of 0.5 °C/min. Five heating/cooling cycles were conducted for each measurement. Data were analyzed using NanoAnalyze (TA Instruments) including normalization for phospholipid concentration and baseline correction.

2.3. Isothermal titration calorimetry (ITC)

ITC experiments were performed using a NanoITC (TA Instruments), consisting of 190 μl sample and reference cells and an injection syringe of 50 μl volume. All ITC scans were obtained at 25 °C, which is above the melting temperature of all studied lipid systems, as confirmed by DSC (supporting Fig. S1); 75 injections (0.66 μl each; waiting time: 900 s) and a stirring rate of 310 rpm were used throughout. Baseline subtraction and data integration were performed with NanoAnalyze (TA Instruments); further analysis was done using Microsoft Excel and Origin 7.0 (OriginLab Corporation, Northampton, MA).

Lipid/LDAO phase diagrams were established via solubilization (S) and reconstitution (R) scans as illustrated in Fig. 2, following previous reports [3,22,23]. In S-experiments, detergent solution was titrated into the lipid solution, whereas the lipid solution was titrated into detergent LDAO solutions in R-experiments. The used concentrations of lipids and detergent in the cell and in the syringe for the two types of experiments are listed in Table S1. The integrated heats Q were background-corrected and used to determine the phase boundaries for a given S or R trajectory. Specifically, the transitions from vesicle to coexistence ranges (SAT) and from coexistence to mixed micelle range (SOL) were derived from the center of error functions fitted to the Q-curves (see example in Fig. 2B). This allowed us to extract phase boundaries for both S and R trajectories with high precision, i.e., with relative errors <1%. However, to account for additional contributions in experimental uncertainty (e.g. instrumental settings), we assigned to each boundary value an uncertainty equal to the average LDAO and lipid concentration increments in the vicinity of the SAT/SOL transitions. This resulted in relative errors of 3 − 7%.

The resulting phase diagrams displayed three ranges (bilayers, coexistence of bilayers and micelles, and only mixed micelles) [16] and were analyzed in terms of a previously reported model [24,23,25,22]. That is, the three ranges are taken to contain different pseudo-phases assuming ideal mixing in all of these pseudo-phases. Then, the SAT

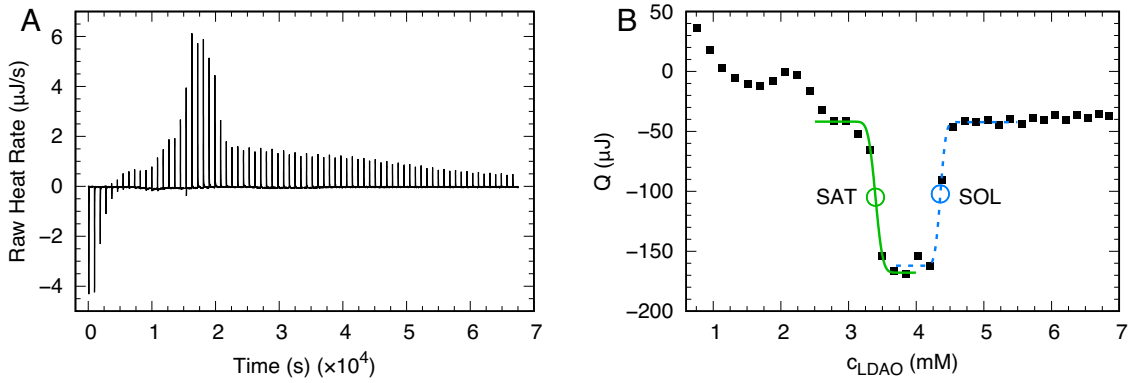

Fig. 2. Solubilization of 1 mM POPG LUVs in TE buffer with 50 mM LDAO; for raw ITC data of other studied lipid systems, see Fig. S2 – S5. Panel A shows the raw thermogram and panel B the corresponding integrated heats. The error functions used to determine the phase boundaries are shown as green solid line for SAT and blue dotted line for SOL. Open circles indicate the transition mid-points. (For interpretation of the references to colour in this figure legend, the reader is referred to the web version of this article.)

and SOL phase boundaries should depend linearly on the lipid concentration c_L

$$\begin{aligned} c_{\mathrm{D}}^{\mathrm{SAT}} &= R_{\mathrm{D}}^{\mathrm{SAT}} \cdot c_{\mathrm{L}} + c_{\mathrm{D}}^{\mathrm{aq,SAT}} \\ c_{\mathrm{D}}^{\mathrm{SOL}} &= R_{\mathrm{D}}^{\mathrm{SOL}} \cdot c_{\mathrm{L}} + c_{\mathrm{D}}^{\mathrm{aq,SOL}}, \end{aligned} \tag{1}$$

where $c_{\mathrm{D}}^{\mathrm{SAT/SOL}}$ corresponds to the maximum detergent concentrations tolerated by bilayers (SAT) or leading to their complete solubilization (SOL), respectively. Further, $R_{\mathrm{D}}^{\mathrm{SAT/SOL}}$ are the slopes of the SAT and SOL pseudo-phase boundaries and $c_{\mathrm{D}}^{\mathrm{aq,\,SAT/SOL}}$ refer to their intercepts, which give the concentration of detergent monomers in the aqueous phase in the presence of lipids in the limit $c_{\mathrm{L}} \to 0$. In the case of ideal mixing, $c_{\mathrm{D}}^{\mathrm{aq,\,SAT}} = c_{\mathrm{D}}^{\mathrm{aq,\,SOL}} = c_{\mathrm{D}}^{\mathrm{aq,\,0}}$ [25]. Although deviations from ideal mixing can be expected for the present systems, we found that $c_{\mathrm{D}}^{\mathrm{aq,\,SOL}}$ was only less then 10% larger than $c_{\mathrm{D}}^{\mathrm{aq,\,SAT}}$ (data not shown). Moreover, analyzing data with either a single common intercept or two intercepts yielded slopes that were comparable within experimental uncertainty. We therefore chose a common intercept, defined as $c_{\mathrm{D}}^{\mathrm{aq,\,0}} = \mathrm{CMC} \cdot R_{\mathrm{D}}^{\mathrm{SOL}}/(1 + R_{\mathrm{D}}^{\mathrm{SOL}})$, for fitting both SAT and SOL boundaries. Here, CMC is the critical micelle concentration, which was reported previously to be 1.94 mM for LDAO at 25 °C [22]. For each data set, we thus performed a linear regression of the SOL boundary with the slope as the single adjustable parameter, and consequently calculated and fixed $c_{\mathrm{D}}^{\mathrm{aq,\,0}}$ in order to fit the SAT boundary. Note that data from S and R experiments were combined to perform each fit.

Fitting the phase boundaries then allows to determine the partitioning coefficients

$$\begin{aligned} K_{\mathrm{L}}^{\mathrm{m\to b}} &= \frac{1 + R_{\mathrm{D}}^{\mathrm{SOL}}}{1 + R_{\mathrm{D}}^{\mathrm{SAT}}} \\ K_{\mathrm{D}}^{\mathrm{m\to b}} &= \frac{R_{\mathrm{D}}^{\mathrm{SAT}}}{R_{\mathrm{D}}^{\mathrm{SOL}}} \cdot K_{\mathrm{L}}^{\mathrm{m\to b}} \\ K_{\mathrm{D}}^{\mathrm{aq\to m}} &= \frac{c_w}{c_{\mathrm{D}}^{\mathrm{aq,0}}} \\ K_{\mathrm{D}}^{\mathrm{aq\to b}} &= \frac{R_{\mathrm{D}}^{\mathrm{SAT}}}{1 + R_{\mathrm{D}}^{\mathrm{SAT}}} \cdot K_{\mathrm{D}}^{\mathrm{aq\to m}}, \end{aligned} \tag{2}$$

where $c_w = 55.5$ M is the molar concentration of water at 25 °C. The individual constants describe partitioning of (i) lipid and detergent between the micellar and the bilayer phase $K_{\mathrm{L}}^{\mathrm{m\to b}}$, and $K_{\mathrm{D}}^{\mathrm{m\to b}}$, respectively; (ii) detergent from the aqueous phase to the micellar phase $K_{\mathrm{D}}^{\mathrm{aq\to m}}$; and (iii) detergent into the bilayer phase $K_{\mathrm{D}}^{\mathrm{aq\to b}}$. The corresponding Gibbs energies of transfer then simply follow from $\Delta G_i^\circ = -k_{\mathrm{B}}T \ln K_i$, where k_{B} is Boltzmann's constant. Error values for $R_{\mathrm{D}}^{\mathrm{SAT}}$ and $R_{\mathrm{D}}^{\mathrm{SOL}}$ were obtained from the error-weighed linear regressions, and then propagated to $c_{\mathrm{D}}^{\mathrm{aq,\,0}}$, K and ΔG° values.

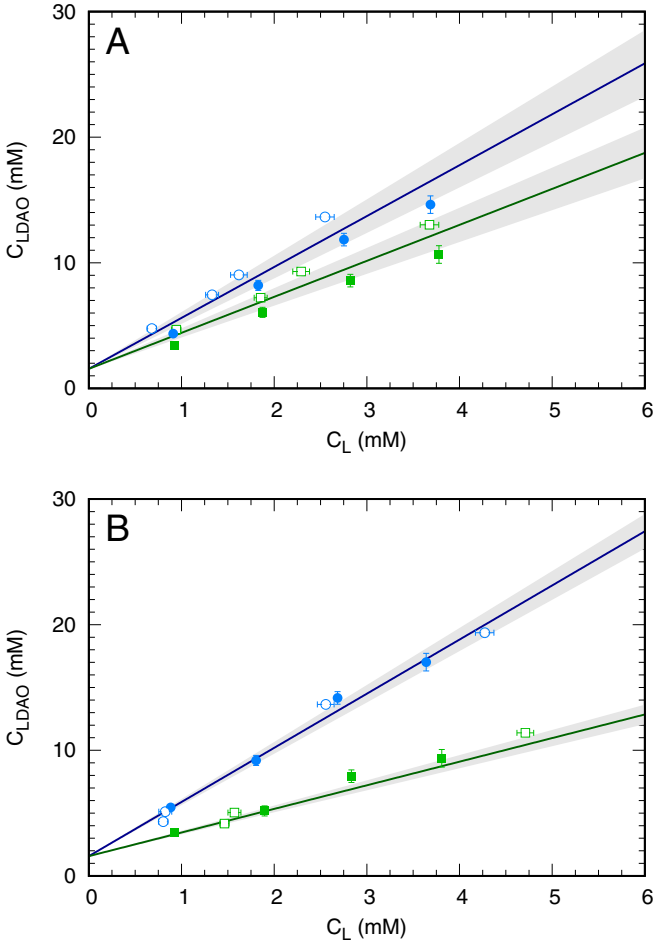

Fig. 3. Phase diagram of pure POPG (A) and POPE:POPG 1:1 mol/mol (B). Blue dots describe solubilization boundaries, while saturation lines correspond to green squares (full and empty symbols refer to solubilization and reconstitution scans, respectively). Data were fitted with Eq. 1 and the gray bands show 95% confidence intervals of the associated uncertainties. (For interpretation of the references to colour in this figure legend, the reader is referred to the web version of this article.)

3. Results

3.1. Interactions with single-component membranes

We started our analysis of lipid/LDAO interactions with single-component LUVs composed of either POPG or TOCL. Fig. 3A shows the phase diagram derived for POPG (for TOCL, see Fig. S6); all results are reported in Table 1. Comparing the slopes of the saturation boundaries ($R_D^{POPG,\ SAT} = 2.94 \pm 0.16$; $R_D^{TOCL,\ SAT} = 5.00 \pm 0.13$) as well as those of the solubilization boundaries ($R_D^{POPG,\ SOL} = 3.9 \pm 0.2$; $R_D^{TOCL,\ SOL} = 11.6 \pm 0.4$) we find that TOCL is able to tolerate more LDAO in bilayers than POPG. In particular, the mole fraction of LDAO needed to solubilize POPG membranes $X_D^{SAT} = R_D^{SAT}/(1 + R_D^{SAT})$ is about 0.62, whereas the lowest detergent mole fraction in micelles required before forming POPG/LDAO bilayers $X_D^{SOL} = R_D^{SOL}/(1 + R_D^{SOL})$ is ~0.81. Instead, $X_D^{SAT} \simeq 0.83$ and $X_D^{SOL} \simeq 0.92$ for TOCL.

The higher stability of TOCL bilayers against LDAO primarily results from the partition coefficients of the lipid from the micellar phase into the bilayer phase (Table 2). Specifically, $K_L^{m\to b}$ of TOCL bilayers is about 1.7 times higher for TOCL than for POPG bilayers. Consequently, the Gibbs energies of transfer $\Delta G_L^{\circ,\ m\to b}$ are more negative for TOCL, i.e. more favorable.

3.2. Interactions with binary and ternary lipid mixtures

In the next step, we studied the interactions of LDAO with POPE/POPG mixtures. Specifically, the mole fractions of POPE in POPG bilayers varied from 25 to 90 mol%. Calorimetric data also revealed linear dependencies of the SAT and SOL boundaries on the lipid concentration, although the co-existence range of micelles and bilayers was broader than for single-component LUVs (Fig. 3B, Fig. S7). Further, the agreement of phase boundaries determined in solubilization and reconstitution experiments was somewhat lower. This led to higher uncertainties for R_D^{SAT} and R_D^{SOL} and, consequently, also for the partition coefficients and the Gibbs energies of transfer (Tables 1,2). Fig. 4A reports the changes in Gibbs energies associated with transferring LDAO or lipids between the three pseudo-phases.

Overall, we observed small but distinct changes in the ΔG_i° values upon changing the lipid composition. By contrast, the Gibbs energy of transferring LDAO to micelles remained virtually constant ($\Delta G_D^{\circ,\ aq\to m} \sim -10.4\ k_BT$). The difference between $\Delta G_D^{\circ,\ aq\to m}$ and $\Delta G_D^{\circ,\ aq\to b}$ was highest at 90 mol% POPE but decreased slightly with increasing POPG content. Strikingly, $\Delta G_L^{\circ,\ m\to b}$ had a maximum for pure POPG bilayers and was lowest at $x_{POPG} = 0.75$, i.e., increased again when lowering POPG content. Repeating experiments with freshly prepared samples reproduced the low $\Delta G_L^{\circ,\ m\to b}$-value at $x_{POPG} = 0.75$. Lipid transfer from micelles to bilayers thus follows non-monotonous behavior, and POPE/POPG (1:3 mol/mol) mixtures are more resilient to LDAO than both pure POPG bilayers and POPE/POPG mixtures enriched in POPE. Most likely, this is due to enthalpic effects related to non-ideal mixing.

To study the behavior of ternary lipid mixtures mimicking bacterial membranes, we kept the mole fraction of POPE constant at 82 mol% and varied the POPG/TOCL molar ratio. Upon increasing the TOCL content, we observed an increase in R_D^{SAT} and R_D^{SOL} (Fig. S8). This indicates that TOCL-enriched membranes are less readily solubilized by LDAO than POPE/POPG/TOCL mixtures with high POPG/TOCL molar ratios, as mirrored also in the decrease of $\Delta G_L^{\circ,\ m\to b}$ with TOCL (Fig. 4B). The Gibbs energies of transfer of LDAO from either micelles or buffer to bilayers ($\Delta G_D^{\circ,\ m\to b}$, $\Delta G_D^{\circ,\ aq\to b}$) in turn do not show significant changes upon increasing TOCL content.

Table 1
Fitting results for LDAO–lipid phase diagrams.

	R_D^{SAT}	R_D^{SOL}	$c_D^{aq,\ 0}$ (mM) [1]
PE:PG			
0:1	2.87 ± 0.17	4.1 ± 0.2	1.56
0.33:1	3.0 ± 0.4	8.5 ± 0.8	1.74
1:1	1.88 ± 0.06	4.31 ± 0.11	1.58
3:1	2.86 ± 0.10	5.4 ± 0.5	1.64
9:1	1.89 ± 0.06	4.48 ± 0.19	1.59
TOCL			
	4.99 ± 0.15	12.0 ± 0.5	1.79
PE:PG:CL			
82:12:6	2.12 ± 0.05	4.9 ± 0.3	1.61
82:9:9	2.06 ± 0.06	4.9 ± 0.3	1.61
82:6:12	1.88 ± 0.11	5.2 ± 0.2	1.63
82:3:15	2.55 ± 0.10	6.2 ± 0.3	1.67

[1] The associated relative standard deviations is <1%.

Table 2
Partition coefficients and Gibbs energies in units of k_BT for LDAO in single-component bilayers.

	$K_D^{aq\to b}$	$K_D^{m\to b}$	$K_L^{m\to b}$
POPG	26,400 ± 700	0.92 ± 0.18	1.31 ± 0.11
TOCL	25,800 ± 200	0.90 ± 0.12	2.17 ± 0.13
	$\Delta G_D^{\circ,\ aq\to b}$	$\Delta G_D^{\circ,\ m\to b}$	$\Delta G_L^{\circ,\ m\to b}$
POPG	−10.18 ± 0.03	0.1 ± 0.2	−0.27 ± 0.09
TOCL	−10.16 ± 0.01	0.20 ± 0.14	−0.77 ± 0.06

3.3. Discussion

We studied the LDAO-induced solubilization thermodynamics of LUVs composed of POPG, TOCL, and mixtures of POPE/POPG and POPE/POPG/TOCL using ITC. All experiments were performed within the fluid lamellar phase (Fig. S1) in order to avoid additional effects from interactions of LDAO with gel-phase membranes [13]. All LDAO-lipid phase diagrams displayed linear dependencies of the saturation and solubilization phase boundaries on lipid concentration and were analyzed in terms of the three-stage model of solubilization [3,22,23]. In particular, we focused exclusively on the transfer Gibbs energies of detergent and lipids between the aqueous, micellar, and bilayer phases.

It is instructive to compare the present results with an analogous study on POPC [22], i.e. same detergent and experimental conditions. While $\Delta G_D^{\circ,\ aq\to b}$ and $\Delta G_D^{\circ,\ m\to b}$ displayed similar values as reported for POPC [22], the other Gibbs energies of transfer showed interesting lipid-specific values. In particular, we find that $\Delta G_{TOCL}^{\circ,\ m\to b} < \Delta G_{POPC}^{\circ,\ m\to b} (= -0.42 k_BT) < \Delta G_{POPG}^{\circ,\ m\to b}$ (Table 2). That is, lipid transfer from micelles to bilayers is least favorable for POPG, followed by POPC and TOCL, or, in other words, the resilience of bilayers against micellization by LDAO follows the order TOCL > POPC > POPG. We did not study pure POPE. However, $\Delta G_L^{\circ,\ m\to b} = -0.69\ k_BT$ in POPE/POPG (9:1 mol/mol) mixtures (Fig. 4A), which is close to the corresponding ΔG°-value for TOCL (Table 2). Thus, we expect that $\Delta G_{POPE}^{\circ,\ m\to b} \approx \Delta G_{TOCL}^{\circ,\ m\to b}$.

The process of micellization of lipid membranes by detergents has been categorized into (i) membrane fragmentation by rapidly inserting and translocating amphiphiles, and (ii) membrane solubilization, i.e., extracting phospholipids from the outer leaflet into micelles, for non-flipping detergents [26]. LDAO rapidly translocates membranes [26] and, hence, most likely will follow the first of the two described scenarios upon partitioning into lipid membranes. The mechanism of vesicle-to-micelle transition is typically discussed as an interplay of monolayer elasticities (bending rigidity, Gaussian curvature modulus, spontaneous curvature) and entropy [17]. In particular, spontaneous monolayer curvature, J_0, i.e., the tendency of lipid monolayers to curve toward or away from the aqueous interface, enters quadratically and, hence, makes a dominant contribution to its elastic behavior. Detergents such as LDAO are well-known to prefer positive curvatures, whereas phospholipids may also have negative J_0-values.

Determination of J_0 is, however, far from trivial. The most commonly applied approximation is to calculate J_0 using shape-based arguments from the average of the intrinsic lipid curvatures, i.e., $J_0 \approx \langle C_0^i \rangle$, where the superscript 'i' refers to a given lipid species. C_0 can be derived

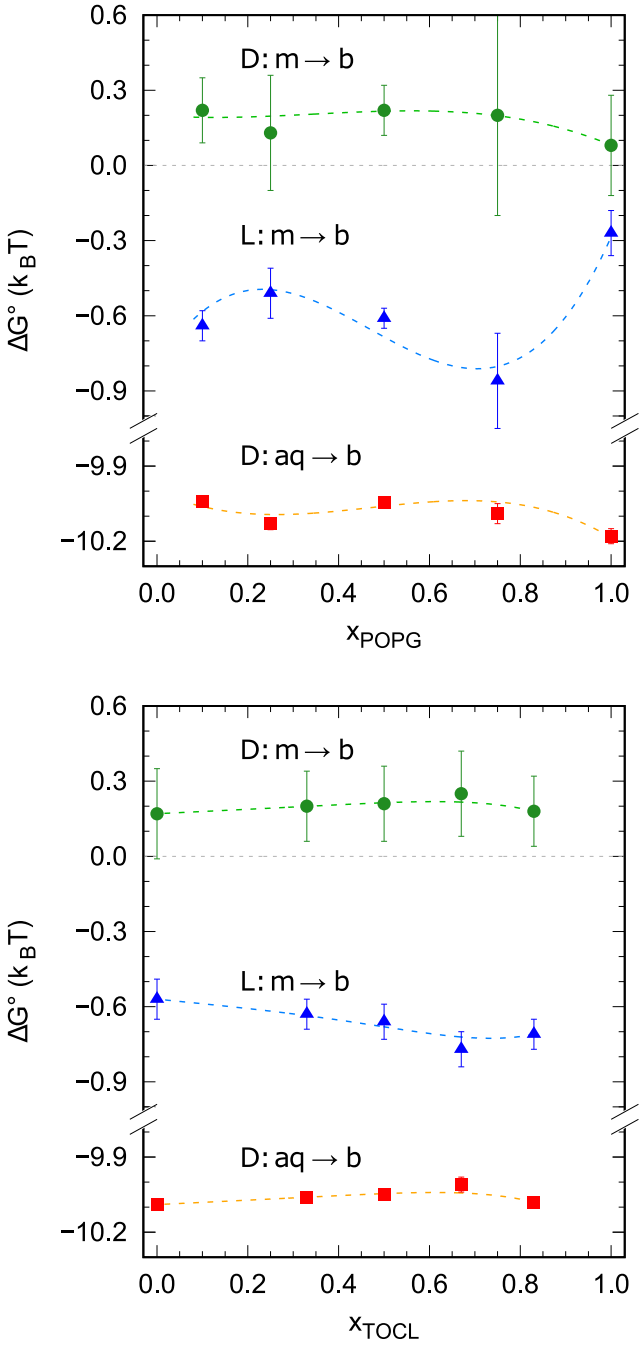

Fig. 4. Gibbs free energies of transfer in POPE/POPG (A) and POPE/POPG/TOCL (B) mixtures as a function of, respectively, POPG molar fraction, x_{POPG}, and TOCL molar fraction, x_{TOCL}. In the latter $x_{POPG} + x_{TOCL} = 1$. $\Delta G_D^{\circ,\ m\to b}$: green dots, $\Delta G_L^{\circ,\ m\to b}$: blue triangles, $\Delta G_D^{\circ,\ aq\to b}$: red squares. Lines are guides for the eye. Free energy values at $x_{TOCL} = 0$ were obtained via a linear interpolation from POPE/POPG systems at $x_{POPG} = 0.18$. (For interpretation of the references to colour in this figure legend, the reader is referred to the web version of this article.)

experimentally from inverted hexagonal phases using small-angle X-ray scattering [27,28] and reflects the curvature property, i.e., shape, of a single lipid molecule. For instance, POPE has a highly negative C_0, consistent with the formation of highly curved inverted hexagonal structures at high temperatures [29]. POPG and TOCL, in turn, do not exhibit such phases, suggesting intrinsic lipid curvatures close to zero. However, pairwise interactions in lipid mixtures containing different headgroups may lead to distinct effects on effective lipid shape leading to so-called non-additive mixing [30]. For example, $J_0 > \langle C_0^i \rangle$ for mixtures enriched in sphingomyelin due to H-bonding [31], but also electrostatic interactions between headgroups in lipid mixtures may lead to significant deviations from the above approximation. Additionally, interactions of lipids with buffer ions may modify J_0 and C_0 [32]. Indeed, we found that the buffer conditions similar to those used here shift intrinsic curvature values of TOCL from slightly positive toward negative values [33], suggesting a screening of electrostatic headgroup repulsion. This means that the effective cardiolipin headgroup area decreases in the presence of buffer ions, 'revealing' a cone-like lipid shape due to the now dominating contributions of the four hydrocarbon chains.

Assuming fully screened electrostatic interactions, we calculated the spontaneous monolayer curvatures of the lipid mixtures J_0^L from the molecular averages of individual lipid curvatures. In particular, we used $C_0^{TOCL} = -0.98\ nm^{-1}$, $C_0^{POPG} = -0.04\ nm^{-1}$, and $C_0^{POPE} = -0.29\ nm^{-1}$ [33]. This allowed us to test whether our systems follow the empirical relation [13].

$$X_D^{SAT} \approx \frac{J_0^L}{J_0^D}, \tag{3}$$

i.e., the molar fraction of detergent needed to solubilize bilayers approximately equals the ratio of spontaneous curvatures of the lipid mixture and detergent. The spontaneous monolayer curvature of LDAO can be estimated from size measurements of their micellar aggregates [34] to be $J_0^D = 0.385\ nm^{-1}$. Plotting X_D^{SAT} as a function of J_0^L/J_0^D (Fig. 5) shows a pronounced non-monotonous behavior, in clear disagreement with Eq. 3. Moreover, J_0^L increases linearly in POPE/POPG mixtures (Fig. 5A, insert), while X_D^{SAT} shows strong fluctuations. Instead, the amount of LDAO needed to solubilize lipid bilayers decreases with the TOCL content in POPE/POPG/TOCL mixtures up to 82:6:12 (mol/mol/mol), but reincreases for 82:3:15 (mol/mol/mol) (Fig. 5B, insert).

We thus conclude that buffer ions do not sufficiently screen non-additive mixing effects emerging from electrostatic interactions. Instead, the non-linear behavior of X_D^{SAT} with either POPG or TOCL concentration suggests that electrostatic interactions between LDAO and POPG/TOCL headgroups dominate the membrane solubilization process. Additionally, we cannot exclude that intermolecular H-bonds due to the presence of POPE, or ion-specific interactions, e.g. preferential adsorption of TRIS, further potentiate non-additive curvature mixing effects.

3.4. Conclusion

Studying the interactions of the zwitterionic detergent LDAO with lipid mixtures of POPE, POPG, and TOCL, we find a qualitative agreement with the three-stage model of detergent-induced membrane solubilization [24]. However, the stability of bilayers composed of these mixtures toward solubilization by LDAO does not quantitatively follow simple shape-based arguments. Instead, our study emphasizes the need to consider additional headgroup interactions, which lead to non-additive curvature mixing effects. For the systems studied here, we speculate that attractive or repulsive electrostatic forces between lipid and detergent molecules significantly stabilize the bilayers. Moreover, the presence of phosphatidylethanolamine might lead to additional contributions from intermolecular H-bonds. More vesicle-to-micelle transition studies of lipid mixtures will be needed to address these issues comprehensively.

Author statement

N.A. and P.P. performed experiments and analyzed data, E.F.S. analyzed data and wrote the paper, S.K. wrote the paper, G.P. designed research and wrote the paper.

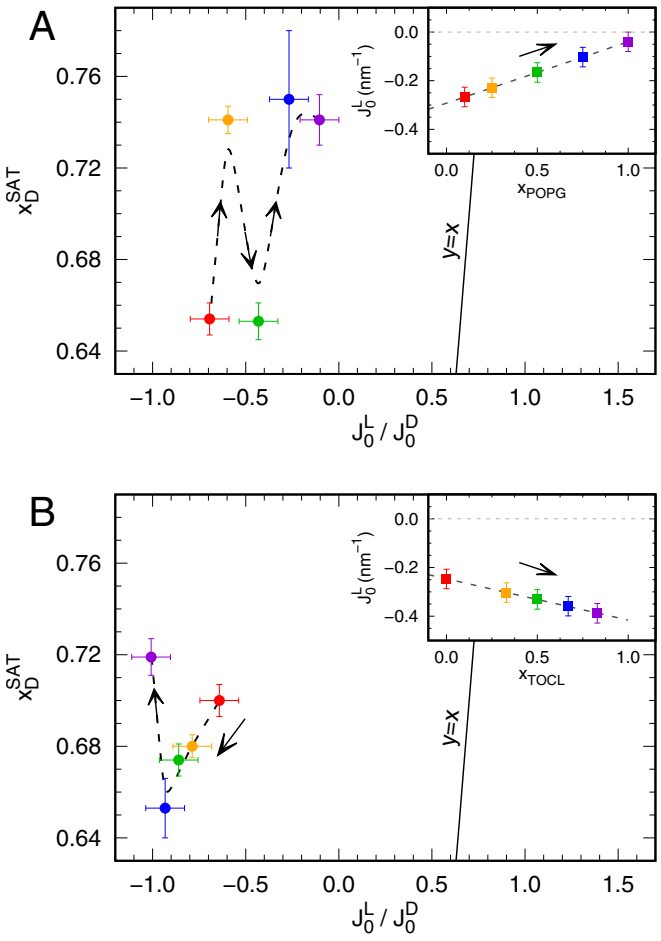

Fig. 5. Evolution of the molar fraction of detergent needed at the saturation boundary, X_D^{SAT}, as a function of the ratio of monolayer spontaneous curvatures of membrane lipids, J_0^L, and LDAO, J_0^D (solid spheres) for POPE/POPG (panel A) and POPE/POPG/TOCL mixtures (panel B). Solid straight lines show the predicted correlation (Eq. 3) [13], whereas dashed lines highlight the effective non linear behaviors. Inserts show the change of spontaneous monolayer curvature, where $X_{TOCL} = 1 - X_{POPG}$ (panel B). Arrows and colour code follow the increase of X_{POPG} (A) and X_{TOCL} (B). The X_D^{SAT} value for $X_{TOCL} = 0$ was obtained applying a linear interpolation of data from panel A.

Declaration of Competing Interest

The authors declare that they have no known competing financial interests or personal relationships that could have appeared to influence the work reported in this paper.

Data availability

Raw ITC and DSC data can be obtained upon reasonable request.

Acknowledgments

This work was supported by the Austrian Science Fund (FWF), grant number P32514.

Appendix A. Supplementary data

Supplementary data to this article can be found online at https://doi.org/10.1016/j.bpc.2023.107002.

References

[1] H.-H. Shen, T. Lithgow, L. Martin, Reconstitution of membrane proteins into model membranes: seeking better ways to retain protein activities, Int. J. Mol. Sci. 14 (1) (2013) 1589–1607, https://doi.org/10.3390/ijms14011589.
[2] I.L. Jørgensen, G.C. Kemmer, T.G. Pomorski, Membrane protein reconstitution into giant unilamellar vesicles: a review on current techniques, Eur. Biophys. J. 46 (2) (2017) 103–119, https://doi.org/10.1007/s00249-016-1155-9.
[3] H. Heerklotz, A.D. Tsamaloukas, S. Keller, Monitoring detergent-mediated solubilization and reconstitution of lipid membranes by isothermal titration calorimetry, Nat. Protoc. 4 (5) (2009) 686–697, https://doi.org/10.1038/nprot.2009.35.
[4] J. Thoma, B.M. Burmann, Fake it till you make it—the pursuit of suitable membrane mimetics for membrane protein biophysics, Int. J. Mol. Sci. 22 (1) (2021) 50, https://doi.org/10.3390/ijms22010050.
[5] H.J. Lee, H.S. Lee, T. Youn, B. Byrne, P.S. Chae, Impact of novel detergents on membrane protein studies, Chem 8 (4) (2022) 980–1013, https://doi.org/10.1016/j.chempr.2022.02.007.
[6] D. Glueck, A. Grethen, M. Das, O.P. Mmeka, E.P. Patallo, A. Meister, R. Rajender, S. Kins, M. Räschle, J. Victor, C. Chu, M. Etzkorn, Z. Köck, F. Bernhard, J. O. Babalola, C. Vargas, S. Keller, Electroneutral polymer nanodiscs enable interference-free probing of membrane proteins in a lipid-bilayer environment, Small 18 (47) (2022), e2202492, https://doi.org/10.1002/smll.202202492.
[7] N. Jahnke, O.O. Krylova, T. Hoomann, C. Vargas, S. Fiedler, P. Pohl, S. Keller, Real-time monitoring of membrane-protein reconstitution by isothermal titration calorimetry, Anal. Chem. 86 (1) (2014) 920–927, https://doi.org/10.1021/ac403723t.
[8] A.G. Lee, Biological membranes: the importance of molecular detail 36 (9) (2011) 493–500, https://doi.org/10.1016/j.tibs.2011.06.007.
[9] M.F. Brown, Soft matter in lipid-protein interactions, Annu. Rev. Biophys. 46 (2017) 379–410, https://doi.org/10.1146/annurev-biophys-070816-033843.
[10] V. Corradi, B.I. Sejdiu, H. Mesa-Galloso, H. Abdizadeh, S.Y. Noskov, S.J. Marrink, D.P. Tieleman, Emerging Diversity in Lipid-Protein Interactions, 2019, https://doi.org/10.1021/acs.chemrev.8b00451.
[11] O. Engberg, D. Ulbricht, V. Döbel, V. Siebert, C. Frie, A. Penk, M.K. Lemberg, D. Huster, Rhomboid-catalyzed intramembrane proteolysis requires hydrophobic matching with the surrounding lipid bilayer 8 (38) (2022) eabq8303, https://doi.org/10.1126/sciadv.abq8303.
[12] G.W. Feigenson, Phase behavior of lipid mixtures, Nat. Chem. Biol. 2 (11) (2006) 560–563, https://doi.org/10.1038/nchembio1106-560.
[13] D. Lichtenberg, H. Ahyayauch, A. Alonso, F.M. Goñi, Detergent solubilization of lipid bilayers: a balance of driving forces, Trends Biochem. Sci. 38 (2) (2013) 85–93, https://doi.org/10.1016/j. tibs.2012.11.005.
[14] A. Hildebrand, K. Beyer, R. Neubert, P. Garidel, A. Blume, Solubilization of negatively charged dppc/dppg liposomes by bile salts, J. Colloid Interface Sci. 279 (2) (2004) 559–571, https://doi.org/10.1016/j.jcis.2004.06.085.
[15] S.T. Clark, M.M. Arras, S.A. Sarles, P.D. Frymier, Lipid shape determination of detergent solubilization in mixed-lipid liposomes, Colloids Surf. B 187 (2020), 110609, https://doi.org/10.1016/j.colsurfb.2019.110609.
[16] A. Helenius, K. Simons, Solubilization of membranes by detergents, Biochim. Biophys. Acta 415 (1) (1975) 29–79, https://doi.org/10.1016/0304-4157(75)90016-7.
[17] M.M. Kozlov, D. Lichtenberg, D. Andelman, Shape of phospholipid/surfactant mixed micelles: cylinders or disks? Theoretical analysis, J. Phys. Chem. B 101 (33) (1997) 6600–6606, https://doi.org/10.1021/jp970295b.
[18] I.M. López-Lara, O. Geiger, Bacterial lipid diversity, Biochim. Biophys. Acta Mol. Cell Biol. Lipids 1862 (11) (2017) 1287–1299, https://doi.org/10.1016/j.bbalip.2016.10.007.
[19] F. Prossnigg, A. Hickel, G. Pabst, K. Lohner, Packing behaviour of two predominant anionic phospholipids of bacterial cytoplasmic membranes, Biophys. Chem. 150 (1–3) (2010) 129–135, https://doi.org/10.1016/j.bpc.2010.04.004.
[20] Navas B. Pozo, K. Lohner, G. Deutsch, E. Sevcsik, K.A. Riske, R. Dimova, P. Garidel, G. Pabst, Composition dependence of vesicle morphology and mixing properties in a bacterial model membrane system, Biochim. Biophys. Acta 1716 (1) (2005) 40–48, https://doi.org/10.1016/j.bbamem.2005.08.003.
[21] G.R. Bartlett, Phosphorus assay in column chromatography, J. Biol. Chem. 234 (3) (1959) 466–468, https://doi.org/10.1016/S0021-9258(18)70226-3.
[22] M. Textor, C. Vargas, S. Keller, Calorimetric quantification of linked equilibria in cyclodextrin/lipid/detergent mixtures for membrane-protein reconstitution 76 (2015) 183–193, https://doi.org/10.1016/j.ymeth.2015.01.002.
[23] M. Herrmann, B. Danielczak, M. Textor, J. Klement, S. Keller, Modulating bilayer mechanical properties to promote the coupled folding and insertion of an integral membrane protein, Eur. Biophys. J. 44 (7) (2015) 503–512, https://doi.org/10.1007/s00249-015-1032-y.
[24] D. Lichtenberg, R.J. Robson, E.A. Dennis, Solubilization of phospholipids by detergents structural and kinetic aspects, Biochim. Biophys. Acta 737 (2) (1983) 285–304, https://doi.org/10.1016/0304-4157(83)90004-7.
[25] S. Keller, H. Heerklotz, N. Jahnke, A. Blume, Thermodynamics of lipid membrane solubilization by sodium dodecyl sulfate, Biophys. J. 90 (12) (2006) 4509–4521, https://doi.org/10.1529/biophysj.105.077867.
[26] U. Kragh-Hansen, M. Le Maire, J.V. Møller, The mechanism of detergent solubilization of liposomes and protein-containing membranes, Biophys. J. 75 (6) (1998) 2932–2946, https://doi.org/10.1016/S0006-3495(98)77735-5.
[27] M.P.K. Frewein, M. Rumetshofer, G. Pabst, Global small-angle scattering data analysis of inverted hexagonal phases, J. Appl. Crystallogr. 52 (Pt 2) (2019) 403–414, https://doi.org/10.1107/S1600576719002760.

[28] M. Kaltenegger, J. Kremser, M.P. Frewein, P. Ziherl, D.J. Bonthuis, G. Pabst, Intrinsic lipid curvatures of mammalian plasma membrane outer leaflet lipids and ceramides, Biochim. Biophys. Acta 1863 (11) (2021), 183709, https://doi.org/10.1016/j.bbamem.2021.183709.
[29] M. Rappolt, A. Hickel, F. Bringezu, K. Lohner, Mechanism of the lamellar/inverse hexagonal phase transition examined by high resolution x-ray diffraction, Biophys. J. 84 (5) (2003) 3111–3122.
[30] A.J. Sodt, R.M. Venable, E. Lyman, R.W. Pastor, Nonadditive compositional curvature energetics of lipid bilayers, Phys. Rev. Lett. 117 (13) (2016), 138104, https://doi.org/10.1103/PhysRevLett.117.138104.
[31] H.J. Lessen, K.C. Sapp, A.H. Beaven, R. Ashkar, A.J. Sodt, Molecular mechanisms of spontaneous curvature and softening in complex lipid bilayer mixtures, Biophys. J. 121 (17) (2022) 3188–3199, https://doi.org/10.1016/j.bpj.2022.07.036.
[32] Y.-F. Chen, K.-Y. Tsang, W.-F. Chang, Z.-A. Fan, Differential dependencies on ca2+ and temperature of the monolayer spontaneous curvatures of dope, dopa and cardiolipin: effects of modulating the strength of the inter-headgroup repulsion, Soft Matter 11 (20) (2015) 4041–4053, https://doi.org/10.1039/c5sm00577a.
[33] P. Reiterer, Ion Specific Effects on Lipid Curvature, Master's thesis, University of Graz, Graz, 2022.
[34] P. Thiyagarajan, D.M. Tiede, Detergent micelle structure and micelle-micelle interactions determined by small-angle neutron scattering under solution conditions used for membrane protein crystallization, J. Phys. Chem. 98 (40) (1994) 10343–10351, https://doi.org/10.1021/j100091a058.